Polymer Chemistry

Accepted Manuscript

ROYAL SOCIETY OF CHEMISTRY

www.rsc.org/polymers

Polymer Chemistry

Polymer Chemistry

Dynamic Article Links ►

Cite this: DOI: 10.1039/c0xx00000x

www.rsc.org/xxxxxx

ARTICLE TYPE

Nitrogen-Enriched Hierarchically Porous Carbons Fabricated by Graphene Aerogel Templated Schiff-base Chemistry for High Performance Electrochemical Capacitors

Xiangwen Yang,[a] Xiaodong Zhuang,[a] Yinjuan Huang,[a] Jianzhong Jiang,[a] Hao Tian,[a] Dongqing Wu,[a] Fan Zhang,[a] Yiyong Mai*[a] and Xinliang Feng*[a,b]

Received (in XXX, XXX) Xth XXXXXXXXX 20XX, Accepted Xth XXXXXXXXX 20XX
DOI: 10.1039/b000000x

This article presents a facile and effective approach towards three-dimensional (3D) graphene-coupled Schiff-base hierarchically porous polymers (GS-HPPs). The method involves the polymerization of melamine and 1,4-phthalaldehyde, yielding Schiff-base porous polymers, on the interconnected macroporous frameworks of 3D graphene areogels. The as-synthesized GS-HPPs possess a hierarchically porous structure containing macro-/meso-/micropores, along with large specific surface areas up to 776 m^2/g and high nitrogen contents up to 36.8 wt%. Consequently, 3D nitrogen-enriched hierarchically porous carbons (N-HPCs) with macro-/meso-/micropores were obtained by the pyrolysis of GS-HPPs at a high temperature of 800 ^oC under nitrogen atmosphere. With a hierarchically porous structure, good thermal stability and high nitrogen-doping contents up to 7.2 wt %, the N-HPCs show high specific capacitance of 335 F/g at 0.1 A/g in 6 M KOH, good capacitance retention with increasing current densities, and outstanding cycling stability. The superior electrochemical performance renders the N-HPCs with great potential as electrode materials for supercapacitors.

Introduction

The problems of aggravating energy and environment pollution are driving us to efficiently use clean and renewable energy sources. The utilization of renewable energy sources generally requires the support of energy storage devices, such as electrochemical capacitors (ECs).[1-3] Since the performance of ECs is strongly governed by the nature of electrode materials, the development of electrochemical materials with high activity and desired structures has been the research focus in the past decade. Carbon materials, such as activated carbons, mesoporous carbons, carbon nanotubes and graphene are the most common and important electrode candidates for ECs.[4-8] In recent years, three-dimensional (3D) electrode materials for ECs based on hierarchically porous carbons with macro-/meso-,[9] meso-/micro-,[10] macro-/micro-,[11] or macro-/meso-/micropores[12] have attracted considerable interest. In these materials, the 3D porous frameworks provide multidimensional electron transport pathways, the macropores act as a bulk buffering reservoir forelectrolytes to minimize the diffusion distances to the interior surfaces of the pores, the mesopores offer a large accessible surface area for ion transport/charge storage, and micropores increase charge accommodation.[9,12]

Monolithic graphene aerogels (GAs) represent a class of new-generation 3D porous carbon materials, which exhibit interconnected macroporous structures, low mass density, large surface-area-to-volume ratio, and high electrical conductivity.[8,9,13-18] Although GAs are devoid of sufficient mesopores and/or micropores, which may improve the efficiency of ion transport/charge storage for ECs, GAs can be used as ideal templates for building up hierarchically porous architectures by integrating mesoporous and/or microporous channels within the interconnected macroporous frameworks of GAs.[9]

Porous polymers with micro-/mesopores, such as hypercrosslinked polymers (HCPs),[19] polymers of intrinsic microporosity (PIMs),[20] and covalent organic frameworks (COFs),[21] have recently drawn great attention owing to their porous features, large surface area, low mass density along with prominent physical properties and potential applications including energy storage and conversion.[22,23] Among various popular strategies for the synthesis of porous polymers, Schiff-base chemistry is a facile and "self-correcting" protocol, which does not require any catalyst and may utilize commercially

[a] *School of Chemical and Chemical Engineering, Shanghai Jiao Tong University, 800 Dongchuan RD, Shanghai 200240, P. R. China; E-mail: mai@sjtu.edu.cn*
[b] *Department of Chemistry and Food Chemistry Technische, Universitaet Dresden, Mommsenstrasse 4, 01062 Dresden, Germany; E-mail: xinliang.feng@tu-dresden.de*
† Electronic Supplementary Information (ESI) available: experimental section, supporting figures and tables. See DOI: 10.1039/b000000x/

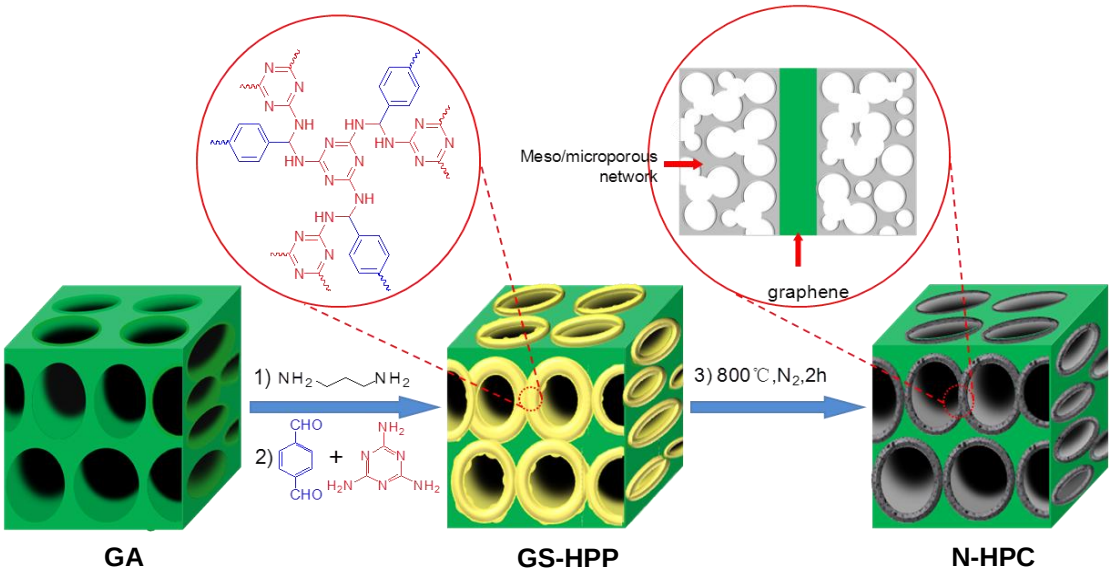

Figure 1. Schematic illustration of the preparation of 3D nitrogen-enriched hierarchically porous carbon (N-HPC).

available and inexpensive monomers.[24-28] Moreover, Schiff-base chemistry may introduce nitrogen composition, which can impart resulting carbon materials with increased surface area, enhanced electronic conductivity, and improved efficiency of charge storage.[26,28]

Apparently, combination of the advantages of both GAs and Schiff-base chemistry may provide a possible pathway for the facile synthesis of 3D nitrogen-enriched hierarchically porous polymers. In this regard, we developed a simple and effective approach towards 3D graphene-coupled Schiff-base hierarchically porous polymers (GS-HPPs) by polymerization of inexpensive monomers (such as melamine and 1,4-phthalaldehyde) on the interconnected macroporous frameworks of GAs without employing catalysts (Figure 1). The resulting GS-HPPs possess a hierarchically porous structure with macropores of sizes ranging from hundreds of nanometers to several micrometers, mesopores of 3–50 nm diameters, and micropores of ca. 1 nm average size. In addition, the incorporation of Schiff-base porous polymers renders the resultant GS-HPPs with large specific surface areas (up to ca. 776 m^2/g) and high nitrogen contents (up to 36.8 wt %). After thermal treatment at 800 ℃ under nitrogen atmosphere, the GS-HPPs were converted into 3D nitrogen-enriched hierarchically porous carbons (N-HPCs) with macro-/meso-/micropores. To the best of our knowledge, the N-HPCs represent the first case of the fabrication of hierarchically porous carbon materials by simple GA templated Schiff-base chemistry. The N-HPCs show good thermal stability and possess large specific surface areas and high nitrogen-doping contents (up to 7.2 wt %). As a result, the N-HPCs exhibit high specific capacitance up to 335 F/g at 0.1 A/g in 6 M KOH electrolyte, good capacity retention with increasing current densities, and outstanding cycling stability. Such electrochemical performance is superior to those of porous carbons prepared from GAs, pyrolyzed porous carbons obtained from Schiff-base porous polymers without GA templates, and many reported 3D graphene or nitrogen-doped porous carbon materials.[8,9,29-34]

Results and Discussion

The strategy for the synthesis of 3D GS-HPPs is presented in Figure 1 and the detail procedures are given in the Electronic Supplementary Information (ESI). Briefly, monolithic GAs were prepared by hydrothermal assembly of graphene oxide (GO, synthesized by a modified Hummer's method) in an aqueous suspension (1.5 mg/mL), followed by a freeze-drying process.[9] Then, aminated GAs (AGAs) were produced by the amidation of the carboxylic acid groups of GAs using 1,3-diaminopropane under the catalysis of N-hydroxysuccinimide (NHS) and N-(3-(dimethylamino)propyl)-N'-ethylcarbodiimide hydrochloride (EDC•HCl) in dimethylformamide (DMF) at room temperature for 1 day. After purification, the obtained AGAs were immersed in an anhydrous dimethyl sulfoxide (DMSO) solution containing estimated amounts of melamine and 1,4-phthalaldehyde; then the mixture was incubated at room temperature for 3 days. Next, a condensation reaction between melamine and 1,4-phthalaldehyde on the interconnected macroporous frameworks of the AGAs was carried out under a catalyst-free condition by refluxing the mixture in DMSO under a nitrogen atmosphere for 3 days. The resultant black bulk products were collected and purified by Soxhlet extraction. Finally, the products were filtered and then dried in vacuum at room temperature overnight. The final products are named as GS-HPP-X (i.e. GS-HPP-5, GS-HPP-10, and GS-HPP-15, respectively), where X represents the weight percentage of aminated GAs in their mixtures with the monomers for polymerization. For comparison, Schiff-base porous polymer was synthesized by the polymerization of melamine and 1,4-phthalaldehyde without involving a GA template under the similar condition; the resulting porous polymer was denoted as PP.

The 3D morphology of the resultant monolithic GAs (the inset of Figure 2a) was characterized by scanning electron microscopy (SEM). An interconnected macroporous framework structure is clearly visualized in the SEM images (Figure 2a). The pore sizes range from hundreds of nanometers to several micrometers.

Nitrogen adsorption-desorption analysis reveals a typical Brunauer–Emmett–Teller (BET) surface area of 201 m^2/g for the GAs (Table 1).

The successful integration of Schiff-base porous polymers on the interconnected macroporous frameworks of GAs was first verified by Fourier transform infrared (FT-IR) spectroscopy (Figure S1, ESI). The bands attributed to the primary amine group of melamine at 3470 and 3420 cm^{-1} (NH_2 stretching) and 1650 cm^{-1} (NH_2 deformation) as well as the bands to the carbonyl group of phthalaldehyde at 2870 (C–H stretching) and 1690 cm^{-1} (C=O stretching) are absent or attenuated greatly in the spectra of the resulting GS-HPPs. The bands corresponding to the quadrant (1556 cm^{-1}) and semicircle stretching (1479 cm^{-1}) of the triazine ring are present. In addition, some signals originated from GAs (e.g. 3430 cm^{-1}, and 1100 cm^{-1}) are also identified in the spectra of GS-HPPs. On the other hand, the elemental analyses reveal high nitrogen contents for GS-HPPs (36.7 wt%, 30.0 wt%, and 24.5 wt% for GS-HPP-5, GS-HPP-10, and GS-HPP-15, respectively. Table 1).

The microstructure of the as-synthesized GS-HPPs was studied by SEM and transmission electron microscopy (TEM). Figure 2 shows the results obtained from GS-HPP-10 as a typical example, while the results from other samples are given in the ESI (Figure S2 and S3). It is obviously seen in Figure 2b that GS-HPPs inherit the interconnected macroporous framework of GAs, and the pore sizes range from hundred of nanometers to several micrometers. Furthermore, polymer layers that are attached uniformly on the macroporous frameworks are clearly observed in the high-magnification SEM images (Figure 2c and d), and the incorporation of the polymer layers is further confirmed by TEM observations (Figure 2e). Element mapping images obtained by scanning TEM (STEM) manifest the homogeneous distributions of carbon and nitrogen in GS-HPPs (Figure 2g-i and Figure S4, ESI). On the other hand, it is known that PP exhibit an amorphous nanoparticle structure (Figure S5, ESI).[24,28] In the present work, no free polymer particles or naked GAs are seen in SEM and TEM images. All of the results strongly suggest that the polymerization of melamine and 1,4-phthalaldehyde takes place on the interconnected macroporous frameworks of GAs.

The hierarchically porous structure of GS-HPPs was confirmed by nitrogen physisorption measurements. The GS-HPPs exhibit type-IV adsorption-desorption isotherms with a hysteresis loop (Figure 2f, Figure S2d and S3d). The isotherms show little uptake at low relative pressures ($P/P_0 < 0.1$), manifesting the existence of micropores. Significant hysteresis at high relative pressures ($P/P_0 > 0.1$) can be seen in the isotherms, indicating the abundance of mesopores. The upward trend at high relative pressures ($P/P_0 > 0.95$) may have originated from the presence of macropores.[35,36] In the inset of Figure 2f, the pore-size distribution (PSD) curve of GS-HPP-10 sample calculated from the corresponding adsorption-desorption isotherm confirms the presence of micropores of ca. 0.6 nm and mesopores of 3–50 nm. Similar pore-size distributions were also obtained for GS-HPP-5 and GS-HPP-15 samples (insets of Figure S2d and S3d). Based on the adsorption-desorption isotherms, the specific surface areas, pore volumes, and average pore sizes (D_{av}) are calculated and listed in Table 1. The specific surface areas and pore volumes of GS-HPPs are up to 776 m^2/g and 2.9 m^3/g, respectively, both of which are much higher than that of GA (ca. 201 m^2/g and 0. 6 m^3/g) and close to that of PP (ca. 795 m^2/g and 2.8 m^3/g).

Table 1. Physical parameters of the samples discussed in this work

Sample [a]	N [b] (wt %)	C [b] (wt %)	S_{BET} [c] [m^2/g]	$S_{Langmuir}$ [m^2/g]	V_{Pore} [d] [cm^3/g]	D_{av} [e] [nm]
GA	NA [f]	NA	201	254	0.6	12.4
PP	NA	NA	795	866	2.8	14.4
GS-HPP-5	36.7	42.4	776	977	2.9	15.0
GS-HPP-10	30.0	45.7	631	798	2.0	12.7
GS-HPP-15	24.5	48.2	424	540	1.0	9.6
PC	NA	NA	431	546	0.8	7.2
N-HPC-5	7.2	72.4	436	511	1.1	9.8
N-HPC-10	6.0	77.9	365	424	0.6	6.6
N-HPC-15	4.8	79.1	290	339	0.5	7.9

[a] PP represents Schiff-base porous polymer from melamine and 1,4-phthalaldehyde; PC means porous carbons prepared by the pyrolysis of PP at 800 °C; GS-HPP-5 represents graphene-coupled Schiff-base hierarchically porous polymers synthesized using 5 wt% aminated GAs during polymerization, the same principle applies to the definition of GS-HPP-10 and GS-HPP-15; N-HPC-5 denotes nitrogen-enriched hierarchically porous carbons produced by the pyrolysis of GS-HPP-5 at 800 °C, the same principle applies to N-HPC-10 and N-HPC-15; [b] weight content measured by elemental analysis; [c] surface area calculated from the N_2 adsorption-desorption isotherms using the BET method; [d] total pore volume at $p/p_0 = 0.99$; [e] average pore size based on the adsorption isotherm; [f] not applicable.

With a hierarchically porous structure and high nitrogen contents, GS-HPPs can serve as exceptional precursors for template-free pyrolysis, producing 3D nitrogen-enriched hierarchically porous carbons (N-HPCs), which have potential application as active electrode materials in supercapacitors.[37] Previous work has demonstrated that 800 °C is an optimum temperature for the pyrolysis of Schiff-base polymers, yielding porous carbons with superb performance for electrochemical capacitors.[24,28,38] This temperature was adopted for carbonization as well in this work. Thermogravimetric analysis (TGA) revealed that at 800 °C, GS-HPPs can be converted into N-HPCs with much higher carbon yields than that of PP (for example, 24.5 wt% vs 9.1 wt% for GS-HPP-10 vs PP, Figure S6, ESI), indicating the pronounced thermal stability of GS-HPPs, attributable to the presence of graphene.[37]

SEM images show that the N-HPCs retain the interconnected macroporous frameworks of GS-HPPs, and the pore sizes range from hundreds of nanometers to several micrometers (Figure 3a, Figure S7a and S8a). In high-magnification SEM graphs (Figure 3b, Figure S7b and S8b), homogeneous distribution of carbon layers on the surfaces of graphene is clearly observed. The alternate dark and light areas in the TEM images confirm the presence of porous carbons that are homogeneously decorated on the graphene surface (Figure 3c, Figure S7c and S8c). The hierarchically porous nature of the N-HPCs was confirmed by nitrogen physisorption measurements. All the N-HPC samples show type-IV adsorption-desorption isotherms (Figure 3d, Figure S7d and S8d). The small uptake at low relative pressures ($P/P_0 < 0.1$) indicates the existence of micropores. The H1-type hysteresis loops at high relative pressures ($0.4 < P/P_0 < 0.95$) manifest that the systems are rich in mesopores. The upward trend at high relative pressures ($P/P_0 > 0.95$) can be attributed to the presence

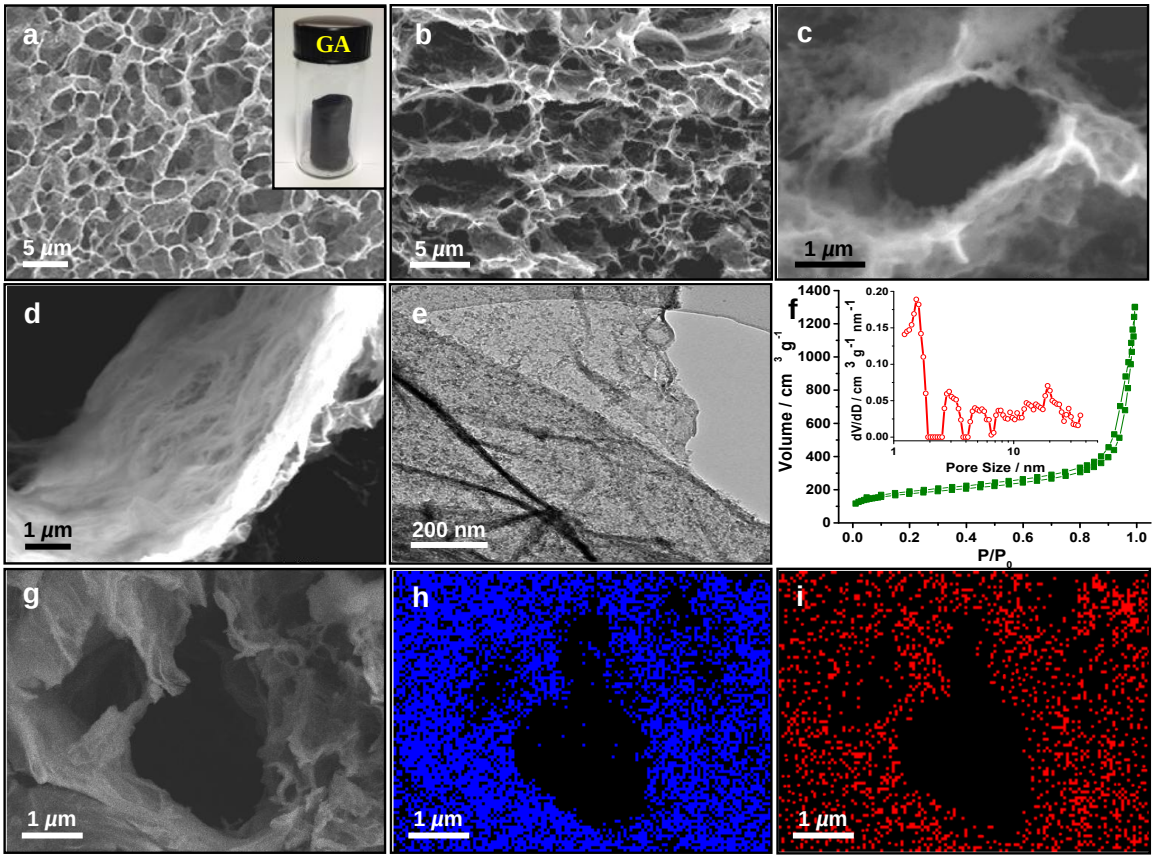

Figure 2. Morphology and microstructure of GA and GS-HPP-10. (a) A typical SEM image of the GA with an interconnected macroporous structure. (b) A SEM image of GS-HPP-10, which inherits the interconnected macroporous structure of GA. (c, d) Local-magnification SEM images of GS-HPP-10, in which homogeneous distribution of Schiff-base polymers is clearly seen. (e) A representative TEM graph of GS-HPP-10. (f) Nitrogen adsorption-desorption isotherm and PSD curve (inset) of GS-HPP-10. (g-i) Typical scanning TEM (STEM) image (g) and the corresponding elemental mapping images of (h) carbon and (i) nitrogen for GS-HPP-10.

of macropores. Specifically, the pore-size distribution (PSD) curve of the GS-HPP-10 sample calculated from the corresponding adsorption-desorption isotherm indicates the presence of micropores of ca. 1.6 nm and mesopores of 3–10 nm (the inset of Figure 3d). Similar pore-size distributions were also obtained for N-HPC-5 and N-HPC-15 (insets of Figure S7d and S8d). The specific surface areas and pore volume of the N-HPCs are up to 436 m^2/g and 1.1 m^3/g, respectively (Table 1), both of which are much higher than those of GA (201 m^2/g and 0.6 m^3/g) and slightly larger than those of PC (431 m^2/g and 0.8 m^3/g). The specific surface areas, pore volumes, and D_{av} of the N-HPCs decrease in comparison to those of the corresponding GS-HPP precursors. This is probably due to the degradation of the Schiff-base polymers and the rearrangement of fragments under the carbonization condition, which might reduce the average pore size and the number of pores in the carbon layers.[37]

The chemical nature of the N-HPCs was investigated by elemental analysis and X-ray photoelectron spectroscopy (XPS). Elemental analyses indicate that the N-HPCs obtained after carbonization have high nitrogen doping contents up to 7.2 wt % (Table 1). On the other hand, in order to understand the variation of different nitrogen species in N-HPCs after the pyrolysis of GS-HPPs, the GS-HPP-10 sample was carbonized under an inert atmosphere at 700, 800, and 900 ℃, respectively. The N1s core-level XPS results reveal high nitrogen contents for GS-HPP-10 and N-HPC-10 samples prepared at various pyrolysis temperatures (Table S1, ESI). The nitrogen content of the GS-HPP-10 (36.1 wt %) and of N-HPC-10 prepared at 800 °C (6.0 wt %) obtained by XPS are in good accordance with those obtained by elemental analysis (30.0 wt% for GS-HPP-10 and 6.0 wt% for

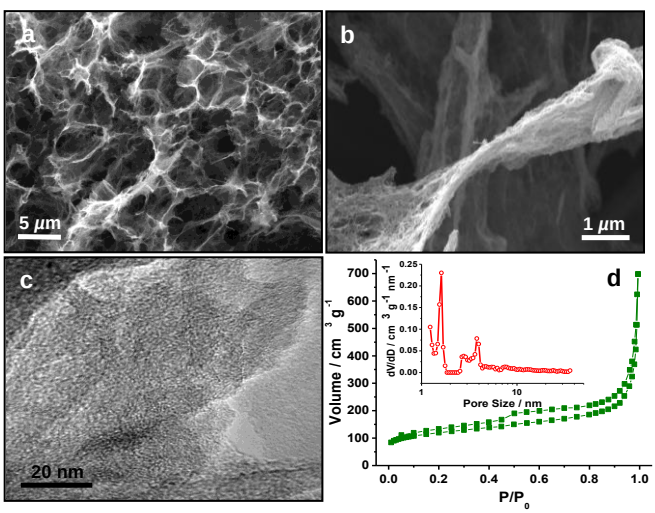

Figure 3. Microstructure and chemical nature of N-HPC-10. (a) A typical SEM image of N-HPC-10, in which the interconnected macroporous framework is obviously seen. (b) A high-magnification SEM photograph, in which carbon layers are clearly observed on graphene surfaces. (c) A representative TEM photograph. (d) Nitrogen adsorption-desorption isotherm and PSD curve (inset).

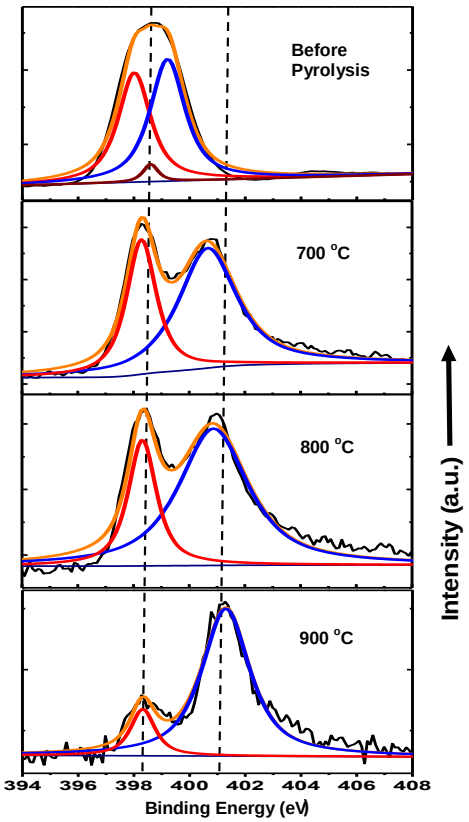

Figure 4. N1s core-level spectra for GS-HPP-10 and N-HPC-10 prepared under different pyrolysis temperatures.

N-HPC-10). Moreover, the nitrogen contents of N-HPC samples decrease as the pyrolysis temperature increases from 700 to 900 ℃ (Table S1). Figure 4 shows the changes of nitrogen species in GS-HPPs and N-HPCs obtained at various pyrolysis temperatures. Before pyrolysis, GS-HPPs possess three types of nitrogen components, which can be assigned to the 1,3,5-triazine units (C–N=C) at ~398.0 eV, the primary amine (C–NH_2) at ~398.6 eV, and the secondary amine (C–NH–C) moieties at ~399.2 eV before pyrolysis;[28] after thermal treatment, the nitrogen species were transformed to pyridine nitrogen (~398.3 eV) and graphitic nitrogen (~401.0 eV).[28] Obviously, the ratio of pyridine N to graphitic N (Table S1) for N-HPCs decreases as the pyrolysis temperature increases, indicating the better thermal stability of graphitic nitrogen against pyridinic nitrogen.

The N-HPC materials with a hierarchically porous structure and a high nitrogen doping content hold promise for applications in electrochemical capacitors. To evaluate the performance of N-HPCs as electrodes for supercapacitors, the electrochemical performances of N-HPCs were examined under alkaline conditions (6 M KOH aqueous solution) using a conventional cell with a three-electrode configuration. Typically, the cyclic voltammetry (CV) curves of N-HPCs measured at a scan rate of 5 mV/s exhibit typical electrical double layer behavior with high capacitances (Figure S9, ESI). Notably, the current density of N-HPC-10 sample is higher than those of other N-HPC samples and PC, indicating a higher specific capacitance for N-HPC-10. The capacitive performance was further studied by galvanostatic charge/discharge measurements (Figure 5a and b). The nearly triangular charge/discharge curves at different current densities

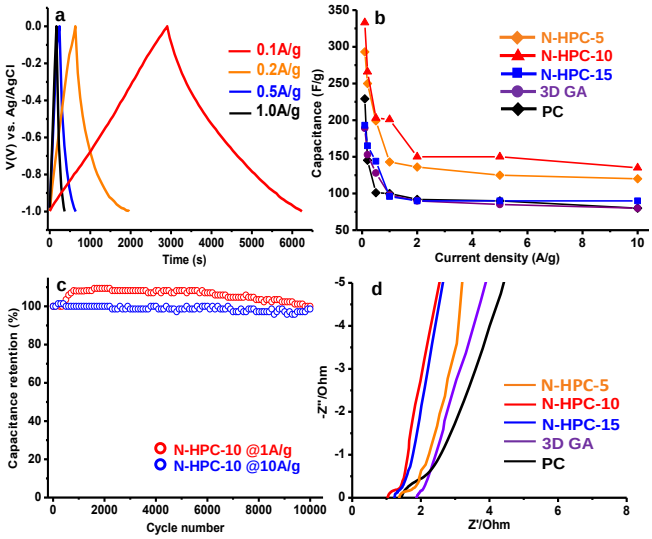

Figure 5. Electrochemical performance of N-HPCs, PC, and GA as electrodes for supercapacitors. (a) Galvanostatic charge/discharge curves for N-HPC-10 at different current densities in 6 M KOH electrolyte. (b) Capacitance retention for N-HPCs, PC, and GA with increasing current density. (c) Cycling stability of N-HPC-10 evaluated at low and high current densities. (d) Nyquist plots for N-HPCs, PC, and GA under open-circuit voltage.

indicate a nearly ideal electrical double layer capacitive behavior and efficient ion transport throughout the N-HPC-10 electrodes (Figure 5a). According to the discharge curve, the specific capacitance of N-HPC-10 is calculated to be 335 F/g at 0.1 A/g, which is superior to those of N-HPC-5 (288 F/g), N-HPC-15 (192 F/g), PC (227 F/g) and GA (187 F/g). It should be emphasized that the specific capacitance of the N-HPC-10 is better than those of many reported heteroatom-doped porous carbons with much larger specific surface areas but without macropores, such as N-doped porous carbon (298 F/g, S_{BET} =1724 m^2/g),[29] B/N-co-doped porous carbon (268 F/g, S_{BET} =894 m2/g),[30] and KOH-activated nitrogen-doped porous carbon (259 F/g, S_{BET} =2970 m^2/g).[31] The capacitance of N-HPC-10 is also higher than those of many reported graphene-based porous carbons, including reduced GO foams (110 F/g),[8] 3D GA-based mesoporous carbon (226 F/g),[9] graphene-based mesoporous carbon nanosheets without macropores (148 F/g),[9] hydrazine reduced graphene hydrogels (220 F/g),[32] nitrogen-doped graphene hydrogels (190 F/g),[33] and hierarchically porous carbon prepared from melamine resin functionalized GO (210 F/g),[34] *etc*.

The N-HPC-10 sample also displays good capacitance retention (Figure 5b). A high specific capacitance of ~150 F/g was obtained for N-HPC-10 at a current density of 2.0 A/g, and this capacitance value retained stably with increasing current densities (till 10 A/g in our experiment). The other two N-HPC samples, GA and PC exhibit similar capacitance retention behavior; however, their specific capacitances are much lower than that of N-HPC-10 within the whole current density window (Figure 5b). The cycling stability of N-HPC-10 was further evaluated by galvanostatic charge-discharge measurement at 1.0 and 10 A/g in a 6 M KOH aqueous solution. Remarkably, almost no capacitance loss is observed for N-HPC-10 after 10,000 cycles at both low and high current densities (Figure 5c). The capacity even enhanced about 10% after 1,000 cycles at the low current density of 1.0 A/g. The increase may be attributed to the

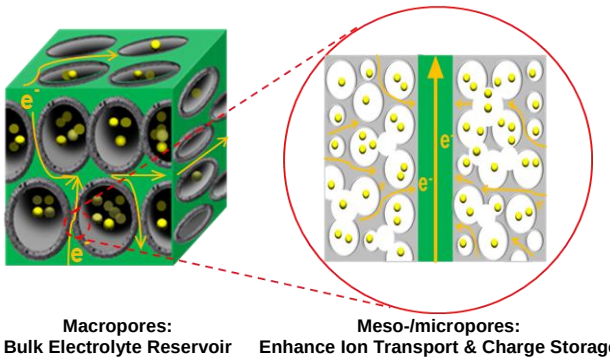

Figure 6. Illustration of the roles of macropores and meso-/micropores for electrochemical capacitors in 3D hierarchically porous framework of N-HPCs.

improvement of ion accessibility in 3D graphene frameworks during the cycling process, which leads to an increased accommodation for charges.[9,12]

In order to understand the superior capacitor performance of N-HPC-10, the conductivity difference between N-HPC-10 and other samples was examined. The impedance spectra are shown in Figure 5d. The semicircle in the impedance curve for N-HPC-10 is found to be smaller than other samples, indicating that the smaller charge-transfer resistance for N-HPC-10. According to the equivalent circuit, the charge-transfer resistance of N-HPC-10 is ~0.3 Ω, which is smaller than those of N-HPC-5, N-HPC-15, GA, and PC (Figure S10 and the caption, ESI). A lowering of the charge-transfer resistance is critical in increasing the specific power output of supercapacitors.[39,40]

The excellent electrochemical performance of N-HPC-10 is considered to arise from its nitrogen-enriched hierarchically porous structure, which provides a synergistic effect of macro- and meso-/micropores (Figure 6). First, the interconnected macropores may buffer ions and thus shorten the diffusion distances from the external electrolyte to the interior surfaces. Second, the meso-/micropores in thin walls, along with the presence of micropores derived from the stacked graphene layers, can enhance ion transport and charge storage. Third, the conductive graphene sheets which construct 3D frameworks may serve as multidimensional pathways to facilitate the transport of electrons in the bulk electrode. On the other hand, among the N-HPC samples, N-HPC-10 shows better capacitor performance than that of N-HPC-5 probably due to the higher content of graphene in N-HPC-10, which may provide better electronic conductivity and thermal stability;[8,9] while N-HPC-5 exhibits better capacitor performance than that of N-HPC-15 owing to the higher surface area and nitrogen doping content, which may render more active sites for ion transport and charge storage.

Conclusions

In this work, we synthesized 3D GS-HPPs via the polymerization of melamine and 1,4-phthalaldehyde, producing Schiff-base micro-/mesoporous polymers, within the interconnected macroporous graphene frameworks. The resultant GS-HPPs possess large specific surface areas up to 776 m^2/g and high nitrogen contents up to 36.8 wt %. 3D N-HPCs were then fabricated by the pyrolysis of GS-HPPs at 800 ℃ under nitrogen atmosphere. The N-HPCs possess a hierarchically porous structure containing macro-/meso-/micropores, good thermal stability and high nitrogen-doping contents up to 7.2 wt %. In particular, the N-HPC-10 sample, fabricated by the pyrolysis of GS-HPP-10 with ca. 10 wt % graphene involved, shows a high specific capacitance of 335 F/g at 0.1 A/g in 6 M KOH with good capacitance retention as well as superior cycling stability with no capacitance loss after 10,000 cycles. Considering the outstanding performance and the facile synthesis approach via GA templated Schiff-base chemistry, the N-HPCs containing macro-/meso-/micropores hold a promise for the application as electrode materials for electrochemical capacitors. Moreover, we believe that the method developed in this work is promising for building up a wide range of other different types of hierarchically porous carbon materials. For instance, GS-HPPs are an ideal template for the fabrication of hierarchically porous carbon/metal oxide hybrids via the incorporation of metal oxide nanoparticles, such as Fe_3O_4 or Co_3O_4, by taking advantage of the affinity of the corresponding metal ion and the nitrogen atoms in GS-HPPs. Employing monomers containing other heteroatoms (such as boron or sulphur) can produce the corresponding heteroatom-doped hierarchically porous carbons. These materials are expected to have potential applications in, e.g. supercapacitors, lithium-ion batteries, and fuel cells.

Acknowledgements

The authors appreciate the financial support from 973 Programs of China (2012CB933404, 2013CB328804, 2013CBA01602 and 2014CB239701), Natural Science Foundation of China (21320102006 and 21304057), Natural Science Foundation of Shanghai City (13ZR1421200), Program for Professor of Special Appointment in Shanghai City (Eastern Scholar), Ph.D. Programs Foundation of Ministry of Education of China for Young Scholars (20130073120088). We also thank the Instrumental Analysis Center of Shanghai Jiao Tong University for some measurements.

References

1 Y. Sun, Q. Wu and G. Shi, *Energy Environ. Sci.*, **2011**, *4*, 1113.
2 S. Yang, R. E. Bachman, X. Feng and K. Müllen, *Acc. Chem. Res.*, **2013**, *46*, 116.
3 Y. Mai, F. Zhang and X. Feng, *Nanoscale*, **2014**, *6*, 106.
4 D. W. Wang, F. Li, M. Liu, G. Q. Lu and H. M. Cheng, *Angew. Chem., Int. Ed.*, **2008**, *47*, 373.
5 Y. W. Zhu, S. Murali, M. D. Stoller, K. J. Ganesh, W. W. Cai, P. J. Ferreira, A. Pirkle, R. M. Wallace, K. A. Cychosz, M. Thommes, D. Su, E. A. Stach and R. S. Ruoff, *Science*, **2011**, *332*, 1537.
6 V. Presser, M. Heon and Y. Gogotsi, *Adv. Funct. Mater.*, **2011**, *21*, 810.
7 Y. Zhai, Y. Dou,; D. Zhao, P. Fulvio, R. Mayes and S. Dai, *Adv. Mater.*, **2011**, *23*, 4828.
8 Z. Niu, J. Chen, H. H. Hng, J. Ma and X. Chen. *Adv. Mater.*, **2012**, *24*, 4144.
9 Z. Wu, Y. Sun, Y. Tan, S. Yang, X. Feng and K. Müllen, *J. Am. Chem. Soc.*, **2012**, *134*, 19532.
10 M. Rose, Y. Korenblit, E. Kockrick, L. Borchardt, M. Oschatz, S. Kaskel and G. Yushin, *Small*, **2011**, *7*, 1108.
11 M. C. Gutierrez, F. Pico, F. Rubio, J. M. Amarilla, F. J. Palomares, M. L. Ferrer, F. del Monte and J. M. Rojo, *J. Mater. Chem.* **2009**, *19*, 1236.
12 H. Jiang, J. Ma and C. Li, *Adv. Mater.* **2012**, *30*, 4197.
13 Z. Tang, S. Shen, J. Zhuang and X. Wang, *Angew. Chem., Int. Ed.*, **2010**, *49*, 4603.

14 Z. Chen, W. Ren, L. Gao, B. Liu, S. Pei and H. Cheng, *Nat. Mater.*, **2011**, *10*, 424.

15 K. S. Novoselov, V.I. Fal'ko, L. Colombo, P. R. Gellert, M. G. Schwab and K. Kim, *Nature*, **2012**, *490*, 192.

16 X. Huang, K. Qian, J. Yang, J. Zhang, L. Li, C. Yu and D. Zhao, *Adv Mater.*, **2012**, *24*, 4419.

17 Y. Zhao, C. Hu, Y. Hu, H. Cheng, G. Shi and L. Qu, *Angew. Chem. Int. Ed.*, **2012**, *51*, 11371.

18 H. Cong, X. Ren, P. Wang and S. Yu, *ACS Nano*, **2012**, *6*, 2693.

19 Y. Luo, B. Li, W. Wang, K. Wu and B. Tan, *Adv. Mater.*, **2012**, *24*, 5703.

20 J. Weber and A. Thomas, *J. Am. Chem. Soc.*, **2008**, *130*, 6334.

21 P. Kuhn, M. Antonietti and A. Thomas, *Angew. Chem. Int. Ed.*, **2008**, *47*, 3450.

22 D. Wu, F. Xu, B. Sun, R. Fu, H. He and K. Matyjaszewski, *Chem. Rev.* **2012**, *112*, 3959.

23 X. Feng, X. Ding and D. Jiang, *Chem. Soc. Rev.* **2012**, *41*, 6010.

24 H. W. Spiess, A. Thomas, X. Feng and K. Müllen, *J. Am. Chem. Soc.* **2009**, *131*, 7216.

25 F. J. Uribe-Romo, C. J. Doonan, H. Furukawa, K. Oisaki and O. M. Yaghi, *J. Am. Chem. Soc.*, **2011**, *133*, 11478.

26 R. Chakrabarty, P. S. Mukherjee and P. J. Stang, *Chem. Rev.*, **2011**, *111*, 6810.

27 E. Preis, C. Widling, G. Brunklaus, J. Schmidt, A. Thomas and U. Scherf, *ACS Macro Lett.*, **2013**, *2*, 380.

28 X. Zhuang, F. Zhang, D. Wu and X. Feng, *Adv. Mater.*, **2014**, *26*, 3081.

29 L. Hao, B. Luo, X. Li, M. Jin, Y. Fang, Z. Tang, Y. Jia, M. Liang, A. Thomas, J. Yang and L. Zhi, *Energ. Environ. Sci.*, **2012**, *5*, 9747.

30 H. Guo and Q. Gao, *J. Power Sources.* **2009**, *186*, 551.

31 H. Wang, Q. Gao and J. Hu, *Microporous Mesoporous Mater.*, **2010**, *131*, 89.

32 L. Zhang and G. Shi, *J. Phys. Chem. C*, **2011**, *115*, 17206.

33 P. Chen, J. Yang, S. Li, Z. Wang, T. Xiao, Y. Qian and S. Yu, *Nano Energy*, **2013**, *2*, 249.

34 J. H. Lee, N. Park, B. G. Kim, D. S. Jung, K. Im, J. Hur and J. W. Choi, *ACS Nano.*, **2013**, *7*, 9366.

35 U. H. F. Bunz, K. Seehafer, F. L. Geyer, M. Bender, I. Braun, E. Smarsly and J. Freudenberg, *Macromol. Rapid Commun.*, **2014**, *35*, 1466.

36 X. Li, S. Yang, J. Sun, P. He, X. Xu and G. Ding, *Carbon*, **2014**, *78*, 38.

37 L. Lai, H. Yang, L. Wang, B. K. Teh, J. Zhong, H. Chou, L. Chen, W. Chen, Z. Shen, R. S. Ruoff and J. Lin, *ACS Nano*, **2012**, *6*, 5941.

38 X. Zhuang, F. Zhang, D. Wu, N. Forler, H. Liang, M. Wagner, D. Gehrig, M. R. Hansen, F. Laquai and X. Feng, *Angew. Chem. Int. Ed.*, **2013**, *52*, 9668.

39 L. Yang, S. Cheng, Y. Ding, X. Zhu, Z. Wang and M. Liu, *Nano Lett.*, **2011**, *12*, 321.

40 L. Hao, X. Li and L. Zhi, *Adv. Mater.*, **2013**, *25*, 3899.

Nitrogen-Enriched Hierarchically Porous Carbons Fabricated by Graphene Aerogel Templated Schiff-base Chemistry for High Performance Electrochemical Capacitors

Xiangwen Yang,[a] Xiaodong Zhuang,[a] Yinjuan Huang,[a] Jianzhong Jiang,[a] Hao Tian,[a] Dongqing Wu,[a] Fan Zhang,[a] Yiyong Mai*[a] and Xinliang Feng*[a,b]

This article presents a facile and effective approach towards three-dimensional nitrogen-enriched hierarchically porous carbons by graphene aerogel templated Schiff-base chemistry.